JOURNAL OF MATERIALS SCIENCE 32 (1997) 5155–5161

Viscoelastic response of solid rocket motor components for service life assessment

S. Y. HO
Weapons Systems Division, Aeronautical and Maritime Research Laboratory, Defence Science and Technology Organisation, P.O. Box 1500, Salisbury, S.A. 5108, Australia

A methodology for determining the response of rocket motor materials and bondlines to thermal loadings by measuring their dynamic mechanical properties is reported. The critical temperatures at which debonding and/or propellant cracking occur and the number of thermal cycles required to induce failure were evaluated. These results were compared with those from instrumented rocket motors subjected to similar thermal loadings. A model, developed for fibre reinforced composites, was applied to the propellant-inhibitor bimaterial obtained from a rocket motor. The internal energy dissipation due to a lack of perfect adhesion at the propellant–inhibitor interface, tan δ_{adh}, was used to give an indication of the failure mode of the bondline (i.e., adhesive failure at the interface or cohesive failure in the propellant) and the bond adhesion parameter, **C**, was related to the bond strength measured by rectangular bond-in-tension tests.

1. Introduction

For solid rocket motors where the critical failure mode is structural failure, i.e., grain cracking and/or debonding, the mechanical behaviour of the various components (e.g., propellant, inhibitor, liner, adhesive) of the motor is very important in the prediction of the service life of the overall rocket motor. In-service rocket motors are often exposed to a wide range of thermal and pressure loading conditions during storage and operation, which can induce fracture in the propellant charge. A particular problem is the susceptibility of the propellant and the propellant–inhibitor interface to cracking and/or debonding under thermal shock conditions (e.g., during air carry where low and high temperature extremes are experienced).

A previous study on the structural analysis of an end burning partially case bonded rocket motor under thermal shock loading conditions, by finite element methods, showed high stress concentrations near the head end of the motor and at the propellant–inhibitor interface adjacent to the adhesive used in the partial case bonding [1]. This was confirmed by radiographs taken after this motor had been subjected to thermal shock tests, which showed axial cracks in/near the propellant–inhibitor interface of the charge adjacent to the motor case bonding [2]. Although the propellant and inhibitor materials were designed to have similar thermal expansion coefficient at ambient temperatures, they can have considerably different rates of expansion/contraction at other temperatures in the operating temperature range of the motor (in particular, below $-10\,^{\circ}C$ and above $+40\,^{\circ}C$ for the motor studied here [2]. Failure at the propellant–inhibitor interface (debonding) is caused by thermal stresses resulting from differences in the thermal expansion coefficients of the different component materials, since the stress free temperature is considerably higher than the storage or operating temperatures. Thus it is important to understand the viscoelastic and mechanical behaviours of the various motor components and the propellant-inhibitor interface under various thermal and pressure loading conditions in order to accurately predict the failure mode of the motor.

Dynamic mechanical thermal analysis (DMTA) is a useful laboratory tool for studying the viscoelastic response and energy dissipation mechanisms of rocket motor materials because only small test specimens are required, and tests can be conducted at the temperatures and low strain levels which are appropriate to the environmental conditions experienced by rocket motors during their service life. Additionally, the effect of ageing time on the viscoelastic response of these materials can be studied [3] by measuring the viscoelastic properties of naturally aged materials over wide temperature and frequency ranges to generate a master frequency curve, using the time–temperature superposition principle, in order to extrapolate the ageing data to a longer time range and thus develop ageing models which may be applicable to service life analysis.

Zorowski and Murayama [4] proposed a mathematical model for interface adhesion in a filament reinforced matrix of lower modulus. Their model, based on theoretical studies [5, 6] of interface dissipation due to slippage in mechanical joints subjected to cyclic loading, assumes a Coulomb friction transfer mechanism and the structure is analysed through a complete cyclic loading, where the area within the resulting hysteresis loop is interpreted as the energy dissipated at the interface. When poor adhesion exists,

0022–2461

energy is dissipated at the interface of the component materials during the cyclic loading. If this interface dissipation could be separated from the other dissipative mechanisms of the composite, DMTA could be used to measure the loss tangent and quantitatively characterize the level of adhesion.

This paper describes the use of DMTA for determining the ageing/thermal shock/thermal cycling behaviour of the solid rocket motor components and interfaces. Zorowski and Murayama's model for interface adhesion, developed for a fibre reinforced composite loaded in tension, is applied to a bimaterial to measure the degree of adhesion at the interface of the component materials. Predictions from DMTA (e.g., likely failure modes, critical temperatures and the number of thermal cycles required to induce failure in the rocket motor materials and interfaces) were compared with stress measurements from instrumented rocket motors subjected to similar environmental loadings.

2. Experimental procedures

Propellant, inhibitor and propellant–inhibitor (P–I) samples were obtained directly from an unaged end burning rocket motor used in an earlier structural analysis study for rocket motor service life prediction [1, 7]. Rectangular samples of 10×8 mm and 1.4 mm thickness (inhibitor and propellant–inhibitor bimaterial) or 3 mm thickness (propellant) were tested in the forced shear mode, using a rectangular torsion geometry, on a Rheometrics dynamic mechanical spectrometer, Model RDA2. The samples were subjected to several thermal shock cycles in the mechanical spectrometer using a programmed time sweep to simulate thermal shock conditions. The programmed time sweep for one thermal shock cycle is as follows: pre-shock: 22 °C for 20 s; cold cycle: -40 °C for 5 h; equilibration at ambient after cold cycle: 22 °C for 30 s; hot cycle: $+55$ °C for 5 h; equilibration at ambient after hot cycle: 22 °C for 30 s.

All measurements were made at a strain level of 0.1% and a frequency of 0.1 rad s^{-1}, and the samples were cycled until failure was detected. The propellant and inhibitor materials are still in the linear elastic region at strain levels up to 1–2%. Thus, the measured non-recoverable damage is mainly due to thermal stresses induced by thermal shock loading.

For the bond adhesion studies, the propellant, inhibitor and propellant–inhibitor bimaterial were machined into $35 \times 12 \times 1.3$ mm bars for testing in tension using a film/fibre fixture on a Rheometrics Solid Analyser, Model RSA2. Measurements were made using a frequency/temperature sweep at a strain level of 0.1%, over the temperature range -40 to $+60$ °C and frequencies of 0.1, 1.0 and 10 rad s^{-1}. The measured tan δ and dynamic modulus, E', values for the bimaterial and component materials were used to calculate the degree of propellant–inhibitor adhesion in the bimaterial using Zorowski and Murayama's model and compared with the propellant–inhibitor bond strength measured by bond-in-tension tests.

3. Results and discussions

Plots of dynamic shear storage, G', and loss, G'', moduli (elastic and viscous components of the material response respectively) and loss tangent (G''/G'), tan δ, as a function of temperature and frequency (0.1–10 rad s^{-1}) for the propellant, inhibitor and P–I

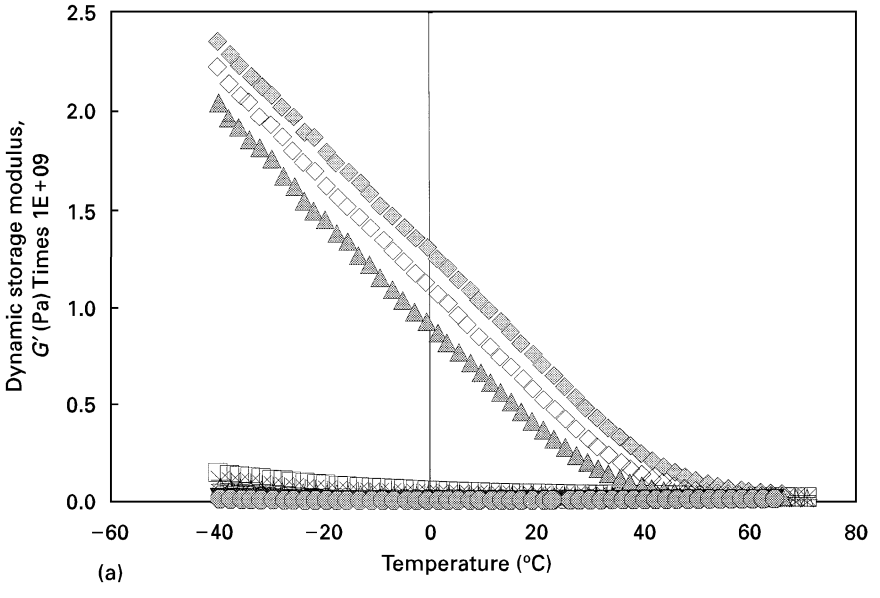

Figure 1 (a) The temperature dependencies of G′ for the propellant at; (◯) 10 rad s^{-1}, (▼) 1 rad s^{-1}, (◍) 0.1 rad s^{-1}, the inhibitor at; (◈) 10 rad s^{-1}, (◇) 1 rad s^{-1}, (◬) 0.1 rad s^{-1} and the propellant – inhibitor bimaterial at; (□) 10 rad s^{-1}, (╳) 1 rad s^{-1} and (☆) 0.1 rad s^{-1}. (b) The temperature dependencies of G″ for the propellant at; (★) 10 rad s^{-1}, (▼) 1 rad s^{-1}, (◯) 0.1 rad s^{-1}, the inhibitor at; (◇) 10 rad s^{-1}, (△) 1 rad s^{-1}, (●) 0.1 rad s^{-1} and the propellant – inhibitor bimaterial at; (◈) 10 rad s^{-1}, (◬) 1 rad s^{-1} and (□) 0.1 rad s^{-1}. (c) The temperature dependencies of tan δ for the propellant at; (★) 10 rad s^{-1}, (▼) 1 rad s^{-1}, (◈) 0.1 rad s^{-1}, the inhibitor at; (▩) 10 rad s^{-1}, (◬) 1 rad s^{-1}, (●) 0.1 rad s^{-1} and the propellant – inhibitor bimaterial at; (◇) 10 rad s^{-1}, (▽) 1 rad s^{-1} and (□) 0.1 rad s^{-1}.

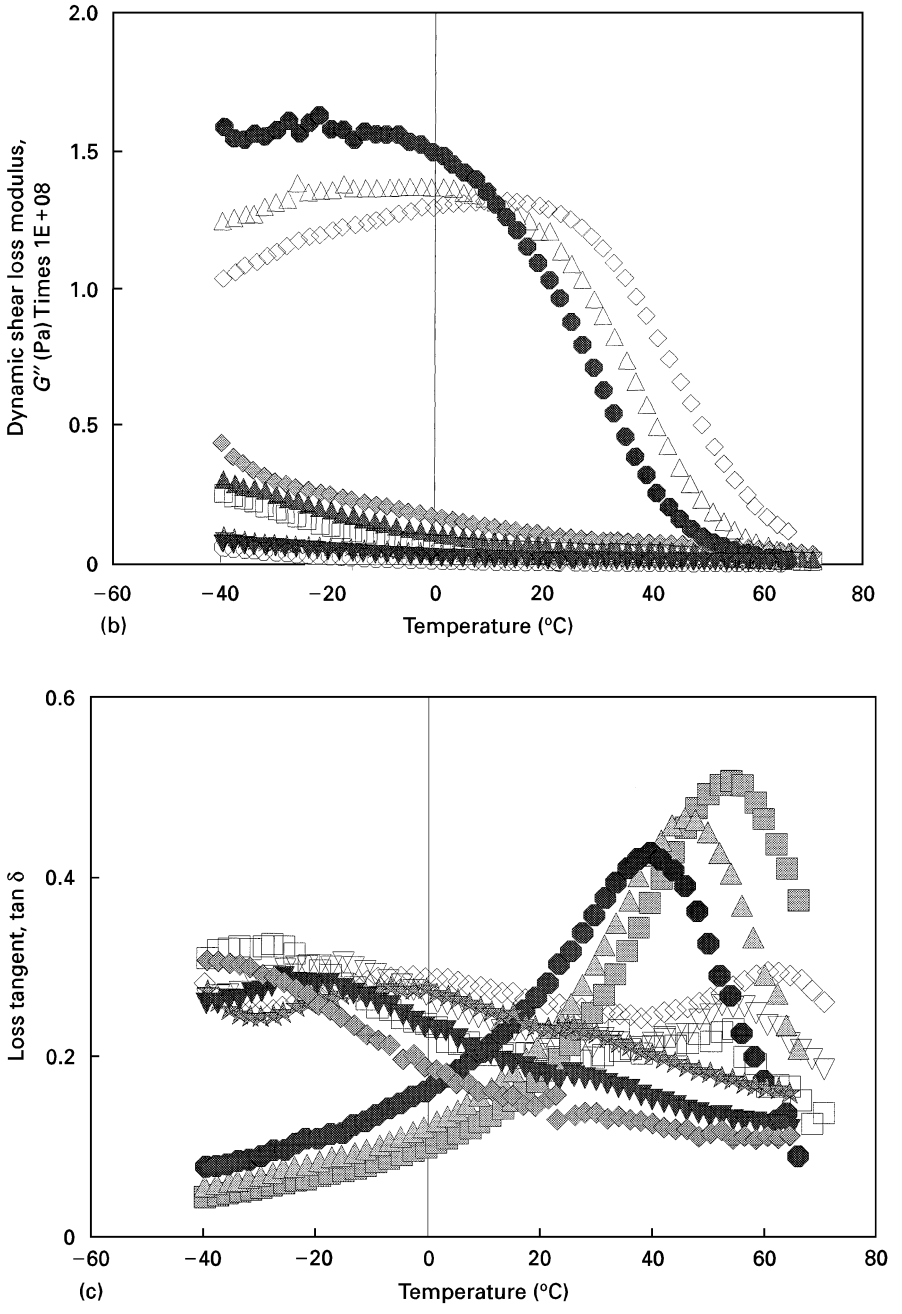

Figure 1 (continued)

bimaterial of the end-burning rocket motor are shown in Fig. 1(a–c). Our results clearly indicate that the modulus of the inhibitor is much higher than those for the propellant and the P–I bimaterial, whereas there is not much difference between the moduli of the propellant and P–I bimaterial over the temperature range -40 to $+60\,^{\circ}C$, suggesting that if failure/cracking in the motor grain occurs it is likely to be at the interface or in the propellant. The G'' and $\tan\delta$ versus temperature plots (Fig. 1(b and c)) show that the inhibitor undergoes a glass transition, T_g, at *ca.* $39\,^{\circ}C$ (estimated from the point where the $\tan\delta$ output was a maximum); i.e., the free volume increases and the inhibitor softens at temperatures above T_g. This may be a critical upper temperature limit for storing this motor as softening of the inhibitor can result in excessive grain deformation and slumping of the grain onto the nozzle, which can lead to catastrophic failure on ignition. The propellant exhibits a small transition, due to relaxation of the hard segments of the hydroxyterminate polybutadiene (HTPB) binder [8], in the temperature range -40 to $-20\,^{\circ}C$.

The component materials and P–I bimaterial were subjected to several thermal shock cycles, using the DMTA, and the changes in shear modulus with each cold and hot cycle are illustrated in Fig. 2(a–c). The temperature change as a function of time are shown in dotted lines. The samples were equilibrated at ambient temperature before each hot or cold cycle. In the analysis, the stress/modulus at thermal equilibrium at the end of each thermal loading was used.

The stress of the P–I bimaterial decreased with each thermal shock cycle, due to mechanical damage. This is illustrated more clearly in Fig. 3(a–c) which show the stress as a function of time for the first five thermal shock cycles, where the changes were most prominent.

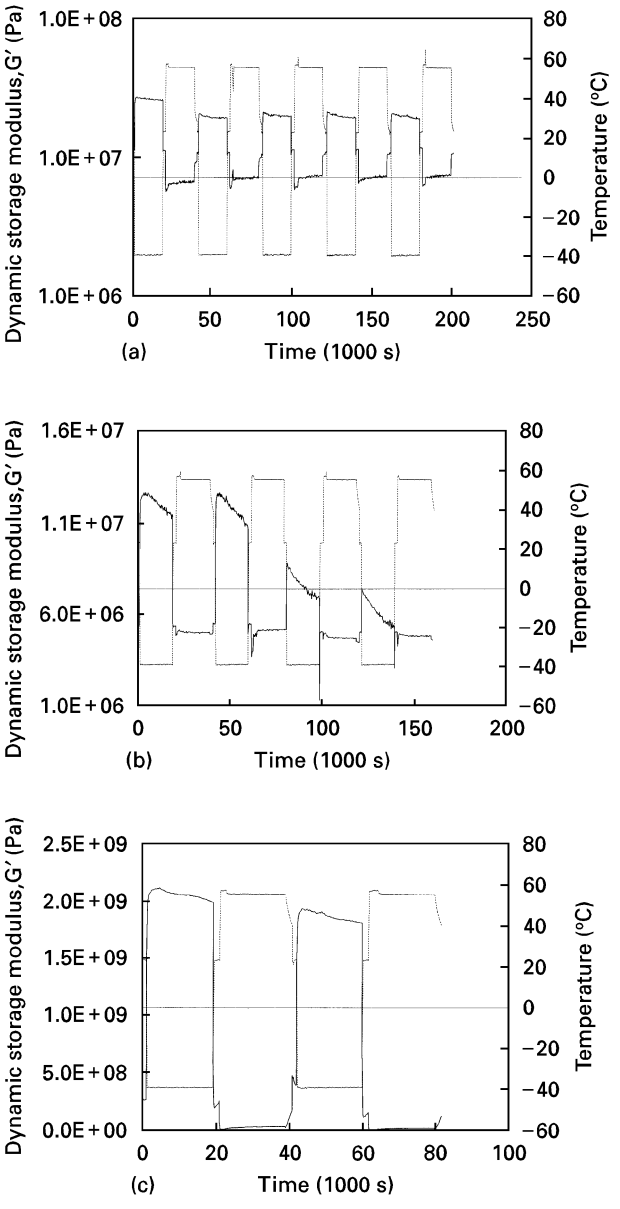

Figure 2 (—) Dynamic storage modulus, (μ) and (- - -) thermocouple temperatures as a function of time for thermal shock test for (a) the propellant – inhibitor bimaterial, (b) the propellant and (c) the inhibitor.

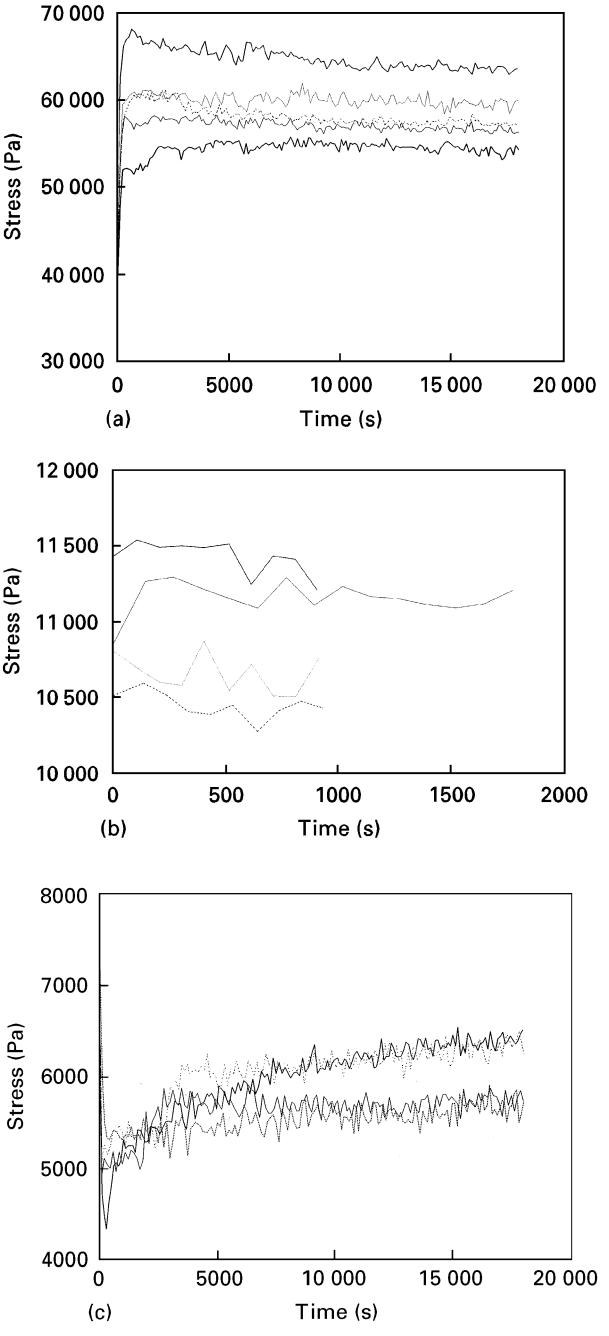

Figure 3 Bondline stresses of the propellant – inhibitor bimaterial for (a) the cold cycles (—) cycle 1, (. . . . .) cycle 2 (—) cycle 3, (—) cycle 4, (----) cycle 5, (b) equilibrium at ambient temperature after cold cycle , (—) Pre thermal shock, (—) equilibration at 22 °C after 1st cold cycle, (. . . . .) Pre 2nd cold cycle, (- - -) Pre 3rd cold cycle, (c) hot cycles, (—) cycle 1, (. . . . .) cycle 3, (—) cycle 4 and (----) cycle 5.

Damage occurred early during the thermal shock experiment, manifested by reductions in the measured stress levels of the sample (see Fig. 3a). For the bimaterial, damage first occurred during the first cold cycle, indicated by a drop in modulus/stress at ambient temperature after the cold cycle (see Fig. 3c; also *cf.* $G'$of the pre-shocked bimaterial with G' at ambient temperature after the first cold cycle). After the third thermal shock cycle, there was a 95% decrease in the modulus and no further reduction in modulus was observed in subsequent cycles. Hence most of the damage occurred during the first three cold cycles and subsequent thermal shock cycles caused no further damage. Mechanical damage was more apparent in the cold cycles than in the hot cycles because at cold temperatures the propellant and inhibitor contract at different rates resulting in tensile stresses which open up the cracks. On the other hand, the differential in thermal expansion during the hot cycle results in compressive stresses which close up the cracks and damage was not apparent until the fourth and subsequent cycles, where most of the damage has already occurred.

The changes in modulus with time when the propellant and inhibitor were subjected to thermal shock loading are illustrated in Fig. 2(b and c). As for the bimaterial, damage was induced during the first thermal shock cycle and completed after the third cycle. However, the reductions in stress levels with each cold cycle were much lower for the inhibitor compared to the propellant and bimaterial. For the propellant, stress relaxation was also observed (see Fig. 2b) and this was very apparent in the cooling cycles,

a consequence of the longer relaxation time at low temperatures (for viscoelastic materials at temperatures above T_g, the stress relaxation time is inversely proportional to temperature) [9].

There is excellent agreement between the trends in the thermal cycling data from DMTA and those from the instrumented rocket motors [2]. For example, damage was more apparent in the cold cycles and the thermal stresses were much higher than those in the hot cycles. The number of thermal shock cycles required to induce failure was also comparable. It should be noted that the number of thermal shock cycles required to cause failure in the rocket motor materials and motor would depend on the minimum and maximum temperatures used in the cold and hot cycles. The thermal loadings used in this study were chosen so that a direct comparison can be made with results from instrumented rocket motors in a previous study. In that study [2], the motors were subjected to environmental loadings which were more severe than what they would normally see in service (i.e., overtest), in order to induce failure in the motor for service life predictions/studies. Our results suggest that DMTA may be used to determine the critical temperatures, in particular lower temperature limits, below which grain cracking and/or debonding will occur.

Over the temperature range -40 to $+60\,^{\circ}C$, the $\tan\delta$ versus temperature plots show the same trends as the variation in thermal expansion coefficient [2] with temperature (cf. Fig. 1c with Fig. 4). This is not surprising since thermal expansion/contraction and mechanical damping ($\tan\delta$) are both related to molecular dynamics or changes in free volume. Thus, the $\tan\delta$ values can be used to give an indication of the temperatures where differentials in the thermal expansion coefficients of the different component materials exist, and therefore the critical temperatures where debonding is likely to occur.

The expected value for $\tan\delta$ as a function of temperature for the P–I bimaterial (assuming the additivity rule and that $\tan\delta$ depends only on the volume fractions of the component materials), if there are no additional damping mechanisms provided by interface

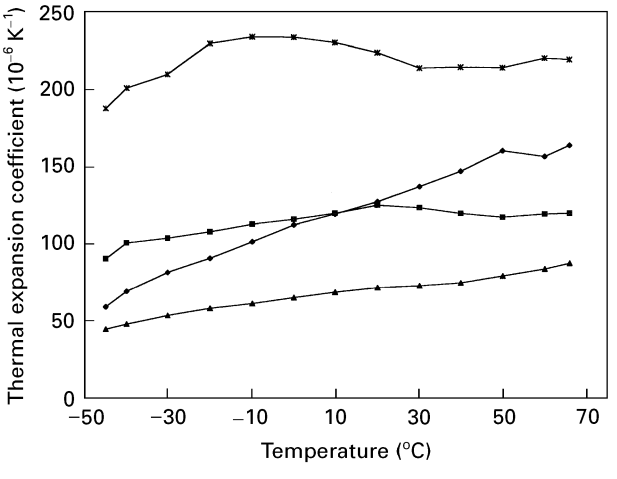

Figure 4 Thermal expansion coefficient as a function of temperature for rocket motor materials (◆) inhibitor, (▲) key, (■) propellant and (✕) insulation.

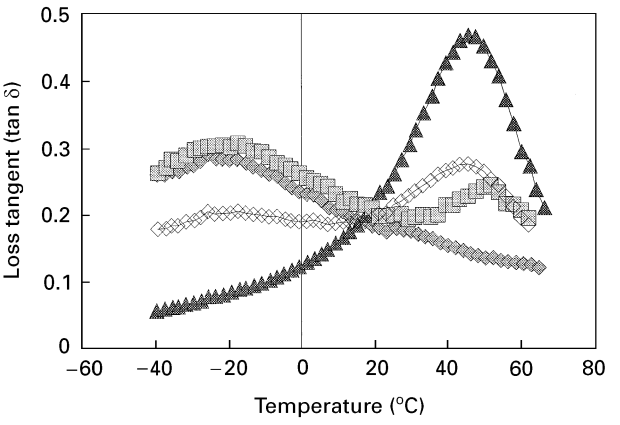

Figure 5 Measured and calculated values for $\tan\delta$ as a function of temperature. Key: (◇) propellant, (△) inhibitor, (▩) propellant – inhibitor bimaterial and (◇) 0.4 inhibitor + 0.6 propellant.

interaction, are shown in Fig. 5. Comparison of the calculated $\tan\delta$ values with those measured experimentally (see Fig. 5) show that the magnitude of $\tan\delta$ was higher than that expected from the additivity rule. Also, the $\tan\delta$ peak of the bimaterial was shifted to a higher temperature (4–8 °C increase) compared to the inhibitor, suggestive of interface interaction. This has also been observed in composites where the filler shifts the $\tan\delta$ peak and T_g to higher temperatures due to interface interaction [8, 10] There are also cases where the fillers increase the damping of the composite, as a result of particle–matrix friction [9].

Zorowski and Murayama [4] developed a theory whereby the total energy dissipation in a composite system under cyclic loading can be separated into a portion that is associated with the viscous properties of the constituent materials and another resulting from lack of perfect adhesion at the matrix interface. They showed that in fibre reinforced composites, the interface dissipation due to poor adhesion can be modelled by:

$$\tan\delta_{adh} = \tan\delta_{exp} - \frac{\tan\delta_f E_f V_f + \tan\delta_m E_m V_m}{E_m V_m + E_f V_f} \quad (1)$$

where $\tan\delta_{adh}$ is the internal energy dissipation due to poor adhesion, $\tan\delta_{exp}$ is the total internal energy dissipation of the system, measured by DMTA, E_f and E_m are the dynamic modulus (E') of the fibre and matrix respectively, and V_f and V_m are the volume fraction of the fibre and matrix respectively. Hence the energy dissipation of the interface, which increases when adhesion is poor, can be determined if the total system energy dissipation and dynamic modulii of the components and volume fractions of the composition are known.

Zorowski and Murayama's [4] experiments on polymer composites showed that a constant bond adhesion parameter, which characterizes the bonding adhesion between the filament and matrix, was obtained when the volume fraction of the fibre was increased from 0.05 to 0.45 (by grinding the matrix surface and reducing the cross-sectional dimensions of the samples) without altering the bonding adhesion. These experiments suggest that their model may also

be applicable to a bimaterial as it is somewhat similar to a composition with a high fibre volume fraction, but has only half the adhesion area.

In the present study, the volume fractions of the component materials of the P–I bimaterial were varied, without altering the interface bonding, by reducing the length of the sample at the propellant end while keeping the cross-sectional area constant. If Zorowski and Murayama's model is valid for bimaterials, then a constant value should be obtained for the bond adhesion parameter, C, which is independent of the volume fraction of the component materials. The constant C characterizes the level and quality of bonding between the constituent materials and is evaluated from the equation [4]:

$$C = \left(\frac{V_p^{1/2} V_i^{1/2}}{E_p V_p + E_i V_i} \left[1 + \frac{V_p E_p}{V_i E_i} \right] \right)^{-1} (\tan \delta_{adh}) \quad (2)$$

where C is the bond adhesion parameter, V_p and V_i are the volume fractions of the propellant and inhibitor in the bimaterial and E_p and E_i are the dynamic modulii of the propellant and inhibitor respectively.

The $\tan \delta_{adh}$ values (loaded in tension), in the temperature range -40 to $+60\,^{\circ}C$, for three P–I bimaterial samples with different volume fractions were calculated using Equation 1. The effect of temperature and volume fraction of the constituent materials on $\tan \delta_{adh}$ and the constant C are illustrated in Table 1 and Figs 6 and 7. The adhesion constant C varies with temperature but at the same temperature it is independent of the volume fraction of the constituents. In the temperature range studied here, the variation from the mean value of the adhesion constant at a given temperature is 2–30% (see Table I). This is well within the experimental error of $\pm 30\%$. Our results clearly show that C is a constant independent of the volume fraction and supports the validity/application of the model of Zorowski and Murayama [4], developed for fibre reinforced composites, to bimaterials.

The bond adhesion parameter, C, at different temperatures are compared with the bond strength values of the P–I bimaterial measured from rectangular bond-in-tension tests (see Fig. 6). As expected, the maximum stress of the propellant–inhibitor bondline decreases with increasing temperature. Additionally, the variation of the bond adhesion constant with temperature follows the same trend as the bond strength – C increases with increasing bond strength. Thus, C can be interpreted as a relative measure of bond strength. However, the DMTA data were *ca.* 2 orders of magnitude higher than those from bond-in-tension tests, due to differences in geometry and loading conditions, etc.

The $\tan \delta_{adh}$ values are indicative of the lack of perfect adhesion at the propellant–inhibitor interface and they vary with temperature (see Fig. 7). As expected, $\tan \delta_{adh}$ was high at temperatures below $-20\,^{\circ}C$, indicating poor adhesion, but was low at temperatures above $0\,^{\circ}C$, indicating good adhesion. Examination of the bond-in-tension samples after testing revealed a change in failure mode with temperature. At $-40\,^{\circ}C$ failure was predominantly adhesive at the interface but at ambient temperature failure was

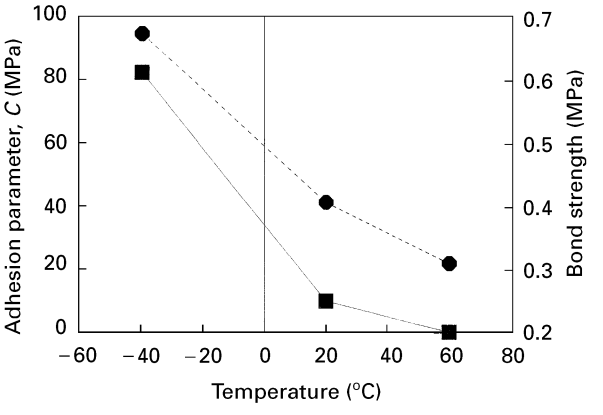

Figure 6 Temperature dependence of (●) bond strength and (■) adhesion parameter.

TABLE I Adhesion constants at various temperatures and volume fractions of component materials.

Temperature (°C)	Volume fraction of propellant	Volume fraction of inhibitor	Adhesion constant, C (dyn cm$^{-2} \times 10^7$)	C, mean value (dyn cm$^{-2} \times 10^7$)	Variation from mean value (%)
−40	0.5	0.5	126		17
	0.6	0.4	115	108	7
	0.8	0.2	82		23
−20	0.5	0.5	120		17
	0.6	0.4	116	102	13
	0.8	0.2	70.5		31
0	0.5	0.5	40.1		28
	0.6	0.4	30.6	31.2	2
	0.8	0.2	22.9		26
20	0.5	0.5	13.6		7
	0.6	0.4	14.4	12.7	13
	0.8	0.2	10.0		21
40	0.5	0.5	16.4		12
	0.6	0.4	16.9	14.5	15
	0.8	0.2	10.6		27

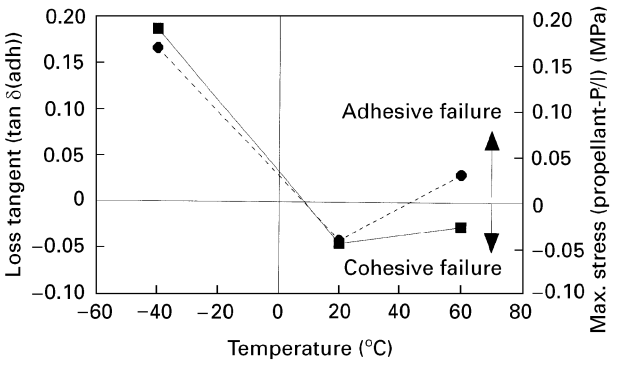

Figure 7 Temperature dependence of (■) $\tan\delta_{adh}$, and (●) difference in maximum stress between propellant and propellant–inhibitor bimaterial.

cohesive in the propellant, and at $+60\,^{\circ}C$ failure was *ca.* 60% cohesive and 40% adhesive. Adhesive failure occurs when the maximum stress of the propellant exceeds that of the bondline whereas, cohesive failure occurs when the maximum stress of the propellant is lower than that of the bondline.

A plot of the difference in maximum stress between the propellant and the bondline versus temperature is also shown in Fig. 7. This difference plot is indicative of whether adhesive or cohesive failure is likely to occur and the correlation of this with the $\tan\delta_{adh}$ values supports the proposal that $\tan\delta_{adh}$ can be used to indicate the type of failure mode, i.e., a high value suggests poor adhesion and failure at the interface whereas a small or negative number suggests that failure is not likely to occur at the interface.

4. Conclusions

The measurement of the dynamic mechanical properties of rocket motor materials and bondlines was found to provide a quick and simple means to evaluate the response of rocket motor materials and bondlines to environmental loadings seen in the motor during its service life. The measured stresses from thermal shock loading showed similar trends to stresses observed in instrumented rocket motors subjected to similar environmental loading conditions. For example, the thermal stresses were much higher in the cold cycles compared to those in the hot cycles and decreased with each thermal cycle due to mechanical damage. After *ca* 3–4 thermal cycles no further damage was observed. These results may be used to determine the critical temperature limits at which debonding and/or grain cracking is likely to occur in the motor. The tan δ values of the constituent materials were found to give an indication of the temperatures where differentials in thermal expansion coefficients exist, and therefore the critical temperatures where debonding is likely to occur.

The model of Zorowski and Murayama for interface adhesion, developed for fibre reinforced composites, was applied to a bimaterial. At the same temperature, the adhesion parameter, C, was a constant, independent of the volume fractions of the constituent materials of the P–I bimaterial. This supports the proposal that the model is also applicable to a bimaterial. There was good qualitative correlation between the adhesion parameter and the maximum stress of the bondline, measured by rectangular bond-in-tension tests, and they showed a similar dependence on temperature. On the other hand, the internal energy dissipation of the bimaterial, $\tan\delta_{adh}$, is indicative of the lack of perfect adhesion at the interface and could be used to predict the likely failure mode (i.e., cohesive failure in the propellant or adhesive failure at the interface).

Acknowledgements

The author thanks Mr K. Ide for providing the thermal expansion coefficient data, Mr T. Ferschl for conducting the bond-in-tension tests, and Mr B. Hamshere for manufacturing and supplying the rocket motor materials.

References

1. E. C. FRANCIS and S. Y. HO, in Proceedings of the 36th AIAA/ASME/ASCE/AHS/ASC Structures, Structural Dynamics, and Materials Conference, AI, New Orleans, LA, USA, April 1995, Paper AIAA 95-1331-CP.
2. S. Y. HO, and P. MACDOWELL, "New service life methodologies for solid propellant rocket motors", Defence Science and Technology Organisation Research Report, DSTO-RR 000. April 1997.
3. S. Y. HO in Proceedings of the 16th meeting of The Technical Cooperation Program, Subgroup W (Conventional Weapons Technology), USA, April 1991.
4. C. F. ZOROWSKI and T. MURAYAMA, in Proc. 1st Int. Conf. on Mech. Behav. of Mater., Vol. 5 (1972) 28.
5. L. E. GOODMAN, *ASME* **36** (1959).
6. A. T. ALPTEKIN Thesis, North Carolina State University, Raleigh. N. C. (1968).
7. S. Y. HO, "Structural Analysis of the Pictor Rocket Motor for Service Life Prediction", in Proceedings of the First Australasian Congress on Applied Mechanics, Melbourne, Vol. 2, 613 (1996).
8. S. Y. HO and C. W. FONG, *J, Mater. Sci.* **22** (1987) 3023.
9. L. E. NIELSEN, in "Mechanical properties of polymers and composites", (Marcel Dekker, New York, 1974).
10. Y. DIAMANT and M. FOLMAN, *Polymer* **20** (1979) 1025.

Received 27 February 1996
and accepted 7 April 1997